Journal of the Korean Physical Society, Vol. 44, No. 5, May 2004, pp. 1033∼1038

Calculation of Radial Profiles of Oxygen Atoms in High-Density Oxygen Discharges

Hyun Jin YOON and Tae Hun CHUNG*
Department of Physics, Dong-A University, Busan 604-714

(Received 2 September 2003)

High-density oxygen plasma discharges are studied by using one-dimensional numerical modeling. A three-fluid equilibrium discharge model is developed for charged species, and a diffusion equation describes the behavior of the oxygen atom. The radial profiles of the neutral atom density and the densities of charged species are calculated. The calculated density profiles are somewhat flatter for lower gas pressures, and the profiles of the negative ions show a stronger density gradient to the wall than those of the positive ions. Overall, the uniformity of the oxygen atoms becomes worse as the pressure increases. The profile of oxygen atom is parabolic (peaked in the plasma center) or hollow, depending on the fractional dissociation. As the fractional dissociation gets larger, the profile becomes hollow, and as it decreases, the profile has a steeper down-slope. The results of the one-dimensional discharge model are expected to be applicable to other discharges with different geometries and electronegative gas chemistries.

PACS numbers: 52.20, 52.25-b, 52.80Pi
Keywords: RF discharge, Oxygen discharge, Radial distribution, One-dimesional modeling, Fluid equation

I. INTRODUCTION

Plasma processing utilizes chemically reactive discharges in order to etch or deposit material onto substrates of interest. Thus, the mechanisms which determine chemically reactive neutral uniformity are of interest. Process uniformity depends strongly on the spatial distribution of both charged and neutral particle densities and velocities, as well as potentials [1, 2]. Process uniformity is a key requirement to enable large wafers or flat panels to be processed by plasma.

Most molecular gases, such as oxygen, chlorine, SF_6, and fluorocarbons, which are used extensively for various applications of plasma processing, produce negative ions in discharges. The presence of negative ions complicates the discharge phenomena. In this study, an oxygen plasma is employed as an example of an electronegative discharge [3–5] since oxygen plasmas have found numerous applications in plasma processing, such as plasma enhanced chemical vapor deposition, reactive sputtering, dry etching of polymers, oxidation, and resist removal of semiconductors.

Atomic oxygen plays an important role in various plasma processes like surface modification of synthetics, surface cleaning, low-temperature growth of silicon dioxide, and etching [1,6,7]. The transfer of these processes developed on the laboratory scale into industrial applications demands large-scale plasma sources with high atomic oxygen densities and uniform distributions.

Mathematical models of plasma generation and transport can be useful for improving our understanding of high-density oxygen plasmas and for investigating the effect of reactor design and operating conditions on plasma uniformity over semiconductor wafers. Two-dimensional direct simulation Monte Carlo studies were performed for the rarefied reactive flow of neutrals and ions in a low-pressure inductively coupled plasma [8,9]. However, these methods require a lot of computational resources. Here, we propose a simple method to predict the spatial profiles of neutral atoms and charged species in high-density plasmas.

For simplicity, we assume that the electronegative plasma consists of three charged species, which are positive ions, negative ions and electrons. An analytic model for a three-component electronegative plasma was developed by Lichtenberg *et al.* [10]. They assumed Boltzmann negative ions and a nearly uniform electron density. An ambipolar diffusion equation for positive ions was set up, and parabolic profiles were obtained. In this study, we calculate the spatial distributions of charged species and neutral oxygen atoms by using a one-dimensional discharge model. The model includes equilibrium fluid equations for charged species and a diffusion equation for oxygen atoms. The assumptions of Boltzmann negative ions and uniform electron density are not necessary. The continuity and momentum balance equations for positive and negative ions are solved

*E-mail: thchung@plasma.donga.ac.kr

numerically.

II. MODEL EQUATIONS

The reactions in high-density oxygen discharges considered in this model are described in Table 1. The rate coefficients are adopted from Ref. [11]. The spatial profiles of densities of charged species and neutral oxygen depend on the reaction rates of the constituents. A three-fluid equilibrium discharge model is developed for charged species, and a diffusion equation describes the behavior of the oxygen atoms. The calculation scheme has two steps. The first step calculates the spatial profiles of the charged species. For simplicity, we only consider the dominant reactions in Table 1, which are recombination, ionization, and dissociative attachment. In this step, the existence of O^+ is neglected. The obtained values of the spatial distributions of charged species are substituted into the diffusion equation for neutral oxygen atoms in the second step. In this step, all reactions listed in Table 1 are considered. The charged species equilibrium model describes positive ions (m_+, e, n_+, T_+), negative ions $(m_-, -e, n_-, T_-)$, and Maxwellian electrons $(m_e, -e, n_e, T_e)$. Ion-ion recombination is assumed to be the dominant loss mechanism for high density oxygen discharges. The electron density is assumed to be the difference between the positive ion density and the negative ion density. The ion continuity and momentum balance equations are

$$\nabla \cdot n_+ \boldsymbol{u}_+ = K_{iz2} n_g n_e - K_{rec2} n_+ n_-, \tag{1}$$

$$\nabla \cdot n_- \boldsymbol{u}_- = K_{att} n_g n_e - K_{rec2} n_+ n_-, \tag{2}$$

$$m_+ n_+ \boldsymbol{u}_+ \cdot \nabla \boldsymbol{u}_+ = n_+ e\boldsymbol{E} - T_+ \nabla n_+ - n_+ m_+ \boldsymbol{u}_+ \nu_+, \tag{3}$$

$$m_- n_- \boldsymbol{u}_- \cdot \nabla \boldsymbol{u}_- = -n_- e\boldsymbol{E} - T_- \nabla n_- - n_- m_- \boldsymbol{u}_- \nu_-, \tag{4}$$

where $\nu_\pm = \sqrt{\frac{8}{\pi}} \frac{\bar{v}_\pm}{\lambda_\pm}$, $\bar{v}_\pm = \sqrt{\frac{T_\pm}{m_\pm}}$, $\boldsymbol{E} = -\frac{T_e}{e} \frac{\nabla n_e}{n_e}$, $n_+ = n_- + n_e$, $\lambda_\pm$ is the ion-neutral mean free path, $\boldsymbol{u}_\pm$ and $\bar{v}_\pm$ are the fluid velocity and the thermal velocity of charged species, $\nu_\pm$ is the momentum transfer collision frequency, $\boldsymbol{E}$ is the electric field, and n_g is the feed gas density.

Although the accurate modeling of the discharge needs two-dimensional or three-dimensional treatment, our analysis will be restricted to the one-dimensional case for simplicity. The radial distribution of charged species can be estimated by employing spherical coordinates. If we neglect the dependence of the densities on the azimuthal and the polar angles, we have

$$\nabla \cdot n\boldsymbol{u} = \frac{d}{dr}[n(r)u_r] + \frac{2}{r} n(r) u_r. \tag{5}$$

We have the non-dimensionalized parameters

$$\tilde{n}_+ = \frac{n_+}{n_{e0}}, \quad \tilde{n}_- = \frac{n_-}{n_{e0}}, \quad \tilde{n}_e = \frac{n_e}{n_{e0}}, \quad \tilde{u}_- = \frac{u_-}{\bar{v}_-},$$

$$\tilde{u}_+ = \frac{u_+}{\bar{v}_+}, \quad k_{iz1} = \frac{K_{iz1} n_g L}{\bar{v}_+}, \quad k_{iz2} = \frac{K_{iz2} n_g L}{\bar{v}_+},$$

$$k_{att} = \frac{K_{att} n_g L}{\bar{v}_+}, \quad k_{disiz} = \frac{K_{disiz} n_g L}{\bar{v}_+},$$

$$k_{diss} = \frac{K_{diss} n_g L}{\bar{v}_+}, \quad k_{de} = \frac{K_{de} n_g L}{\bar{v}_+},$$

$$k_{rec1} = \frac{K_{rec1} n_{+0} L}{\bar{v}_+}, \quad k_{rec2} = \frac{K_{rec2} n_{+0} L}{\bar{v}_+},$$

$$\xi = \frac{r}{L}, \quad \frac{d}{dr} = \frac{d\xi}{dr}\frac{d}{d\xi} = \frac{1}{L}\frac{d}{d\xi},$$

where L is the system length. The reaction rate constants (K) are given in Arrhenius form in Table 1.

The non-dimensionalized ion continuity and momentum equations are

$$\frac{d(\tilde{n}_+ \tilde{u}_+)}{d\xi} + \frac{2\tilde{n}_+ \tilde{u}_+}{\xi} = k_{iz2} \tilde{n}_e - k_{rec2} \frac{\tilde{n}_+ \tilde{n}_-}{1+\alpha_0}, \tag{6}$$

$$\frac{d(\tilde{n}_- \tilde{u}_-)}{d\xi} + \frac{2\tilde{n}_- \tilde{u}_-}{\xi} = k_{att} \tilde{n}_e - k_{rec2} \frac{\tilde{n}_+ \tilde{n}_-}{1+\alpha_0}, \tag{7}$$

$$\frac{d\tilde{n}_+}{d\xi} = \tilde{n}_+ \gamma_+ f - \frac{\tilde{n}_+ \tilde{u}_+}{d_+} - \tilde{n}_+ \tilde{u}_+ \frac{d\tilde{u}_+}{d\xi}, \tag{8}$$

$$\frac{d\tilde{n}_-}{d\xi} = -\tilde{n}_- \gamma_- f - \frac{\tilde{n}_- \tilde{u}_-}{d_-}, \tag{9}$$

where $\alpha_0 = n_{-0}/n_{e0}$, $\gamma_\pm = T_e/T_\pm$, $d_\pm = D_\pm/(\nu_\pm L)$, $D_\pm = T_\pm/(m_\pm \nu_\pm)$, and

$$f = \frac{\frac{u_+}{d_+} - \frac{u_-}{d_-}(1-u_+^2)\frac{n_-}{n_e+n_-} + \frac{k_z u_+ n_e}{n_e+n_-} - \frac{k_r u_+ n_-}{1+\alpha_0}}{\gamma_+ + \frac{(1-u_+^2)(n_e+\gamma_- n_-)}{n_e+n_-}}. \tag{10}$$

The convective term in the negative ion momentum equation has been neglected.

The spatial profile of atomic oxygen depends on the source rate and the sink rate of atomic oxygen. Based on the reactions in Table 1, we can estimate this profile. We simplify the problem by assuming a uniform distribution of fractional dissociation, isothermal gases, and a uniform electron temperature. It should be noted that reactions with O^+ are considered because efficient production of O^+ is realized in high-density oxygen discharges [12]. The diffusion equation of neutral atoms is written as

$$\begin{aligned} -D_O \nabla^2 n_O = {} & K_{att} n_e n_{O_2} + K_{disiz} n_e n_{O_2} \\ & + 2K_{diss} n_e n_{O_2} + K_{rec1} n_{O_2^+} n_- \\ & + K_{rec2} n_{O^+} n_- + K_{de} n_e n_- - K_{iz1} n_e n_O, \end{aligned} \tag{11}$$

where D_O is the atomic oxygen diffusion coefficient and n_O is the atomic oxygen density. The non-dimensionalized neutral diffusion equation is

$$-d_O \left[\frac{d^2 \tilde{n}_O}{d\xi^2} + \frac{2}{\xi} \frac{d\tilde{n}_O}{d\xi} \right]$$

Table 1. Model reaction set for an oxygen plasma.

Reactions				Rate coefficients	units
Ionization 2	$e + O_2$	$\rightarrow$	${O_2}^+ + 2e$	$K_{iz2} = 9.0 \times 10^{-16} T_e^2 \exp(-\frac{12.6}{T_e})$	$m^{-3}s^{-1}$
Dissociative Attachment	$e + O_2$	$\rightarrow$	$O^- + O$	$K_{att} = 8.8 \times 10^{-17} \exp(-\frac{4.4}{T_e})$	$m^{-3}s^{-1}$
Recombination 2	${O_2}^+ + O^-$	$\rightarrow$	$O_2 + O$	$K_{rec2} = 1.5 \times 10^{-13} \left(\frac{300}{T_g}\right)^{0.5}$	$m^{-3}s^{-1}$
Recombination 1	$O^- + O^+$	$\rightarrow$	$O_2 + O$	$K_{rec1} = 2.5 \times 10^{-13} \left(\frac{300}{T_g}\right)^{0.5}$	$m^{-3}s^{-1}$
Detachment	$e + O^-$	$\rightarrow$	$O + 2e$	$K_{det} = 2.0 \times 10^{-13} \exp(-\frac{5.5}{T_e})$	$m^{-3}s^{-1}$
Dissociative Ionization	$e + O_2$	$\rightarrow$	$O + O^+ + 2e$	$K_{disiz} = 5.3 \times 10^{-16} T_e^{0.9} \exp(-\frac{20}{T_e})$	$m^{-3}s^{-1}$
Ionization 1	$e + O$	$\rightarrow$	$O^+ + 2e$	$K_{iz1} = 9.0 \times 10^{-15} T_e^{0.7} \exp(-\frac{13.6}{T_e})$	$m^{-3}s^{-1}$
Dissociation	$e + O_2$	$\rightarrow$	$2O + e$	$K_{diss} = 4.2 \times 10^{-15} \exp(-\frac{5.6}{T_e})$	$m^{-3}s^{-1}$

$$= \left[\left(\frac{1-X}{X}\right)(k_{att} - k_{disiz} + 2k_{diss}) - k_{iz1}\right]\tilde{n}_e\tilde{n}_O + \frac{n_{e0}}{n_g}\left[\frac{1}{\alpha_0+1}\left(k_{rec2} + \frac{X}{1-X}k_{rec1}\right)\tilde{n}_+\tilde{n}_- + k_{de}\tilde{n}_e\tilde{n}_-\right] \quad (12)$$

where $\tilde{n}_O = n_O/n_g$, $d_O = D_O/\nu_O L$, and the fractional dissociation X is defined as $\frac{n_O}{n_O+n_{O_2}}$. Therefore, we have $n_{O_2} = (1-X)n_g$ and $n_O = Xn_g$, and we assume that $\frac{n_O}{n_{O_2}} \simeq \frac{n_{O^+}}{n_{O_2^+}}$ [13], $n_+ = n_{O_2^+} + n_{O^+}$, and $n_- = n_{O^-}$.

The fractional dissociation X can be estimated if we consider only the dominant generation and destruction mechanisms for oxygen atoms:

$$2K_{diss}n_e n_{O_2} = O_{loss}n_O \ , \quad (13)$$

where $O_{loss} = \gamma_{rec}\frac{1}{4}\frac{v_{th}A}{V}$ is the oxygen atom loss rate to the wall, $v_{th} = \left(\frac{8k_BT_g}{\pi m_O}\right)^{\frac{1}{2}}$ is the thermal velocity of the neutral atom, γ_{rec} is the surface recombination rate, and V and A are the volume and the surface area of the chamber. Equation (13) becomes

$$2K_{diss}(1-X)n_e = \frac{1}{4}\gamma_{rec}\frac{v_{th}}{\tilde{L}}X \ , \quad (14)$$

where $\tilde{L}(= V/A)$ is the characteristic length scale of the plasma. Equation (14) gives

$$X = \frac{8n_e\tilde{L}K_{diss}}{8n_e\tilde{L}K_{diss} + \gamma_{rec}v_{th}} \ . \quad (15)$$

The electron density, the electron temperature, γ_{rec}, and T_g (temperature of atomic oxygen gas), can give estimate of X. The fractional dissociation X has values larger than 0.6 for most high-density oxygen plasmas.

Charged particle densities and the neutral oxygen atom density are calculated from Eqs. (6) to (10) and Eq. (12) by using the fourth-order Runge-Kutta method [14] with the initial values $\tilde{n}_{e0} = 1$, $\tilde{n}_{-0} = \alpha_0$, and $\tilde{u}_+ = \tilde{u}_- = 0$ at the center of the chamber (ξ=0). The input values of $n_{+0}, \alpha_0, T_+, T_-, T_e, L$, and n_g must be supplied. These values can be obtained by global modeling for a given pressure and input power condition [13]. The formulation here can be extended to two-dimensional and three-dimensional calculations and simulates real systems more accurately. Throughout this study, $T_e = 3$ eV is used, and X=0.7 is chosen unless otherwise stated.

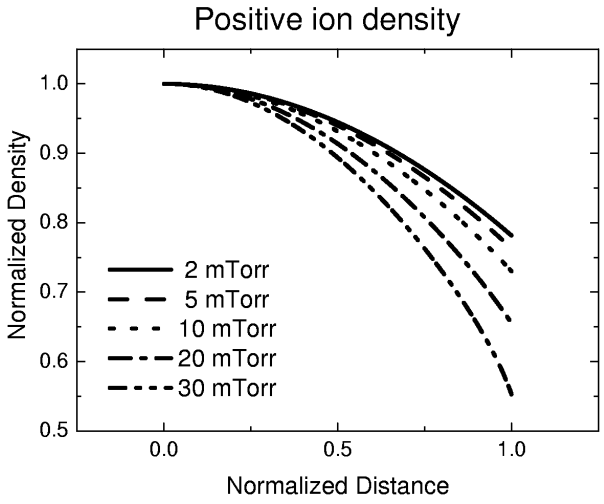

Fig. 1. Density profiles of positive ions at various pressures (p = 2, 5, 10, 20, 30 mTorr).

III. RESULTS AND DISCUSSION

Figure 1 shows the density profiles of positive ions at various pressures. The calculated values are normalized by the center values (the initial values). The calculated density profiles are somewhat flatter for lower gas pressures. This may be due to the neglect of the electropositive edge region in the calculations. The boundary condition on the particle density at the wall is not applied since this model describes the plasma bulk region only. Near the wall, presheath and sheath regions exist where quasi-neutrality of charge and the Boltzmann relation of electrons are not valid. As can be seen in Fig. 2, the density profiles of negative ions have steeper slopes than

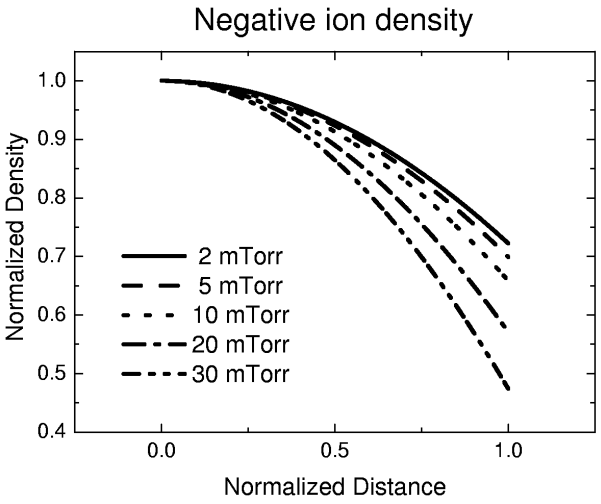

Fig. 2. Density profiles of negative ions at various pressures (p = 2, 5, 10, 20, 30 mTorr).

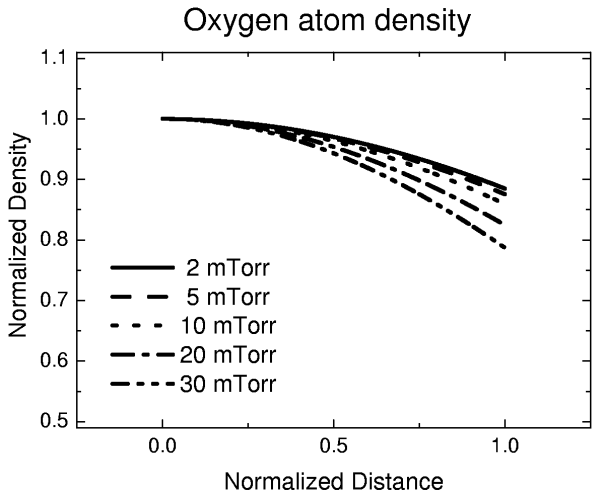

Fig. 3. Density profiles of oxygen atoms at various pressures (p = 2, 5, 10, 20, 30 mTorr).

those of positive ions along the distance. In other words, the profiles of negative ions show stronger density gradients to the wall than those of positive ions. Since the electron density is the difference between the positive ion density and the negative ion density, it has a profile similar to those of the positive and the negative ions. In a helicon oxygen discharge, the plasma uniformity has been observed to be degraded at higher pressure [7].

The main drawback of this model is that the density profiles are not accurate near the wall since the formulation of this study does not describe the behavior of charged species in the electropositve region and the sheath region. In the case of a capacitively coupled plasma for which a spherical coordinate system is difficult to apply, this causes a significant error in estimating the density profiles. However, in high-density plasma sources, such as an inductively coupled plasma and a helicon, the discrepancies in the density profiles may not be significant, especially so in large-area sources.

In Fig. 3, we can observe that the profile of oxygen atoms is peaked in the center, in contrast to that of the argon discharge. The feed neutral gas itself experiences rapid depletion (ion-pumping effect). Because this removal rate is much faster than the rate of thermal neutral diffusion from the walls or gas injection sources, the neutral density in the central portion of the plasma can be significantly reduced [7,15]. The neutral atoms in an oxygen discharge has a behavior different from that in the monatomic feed gas case like argon. The calculated radial distributions of oxygen atoms are in agreement with the experimental results [1,7]. Overall, the uniformity of oxygen atoms becomes worse as the pressure increases. In a microwave oxygen discharge with increasing pressure, the atomic oxygen homogeneity is observed to degrade [16]. At lower pressure, the oxygen atom density is nearly homogeneous due to the greater diffusion length [16]. The calculated profile of oxygen atoms compares

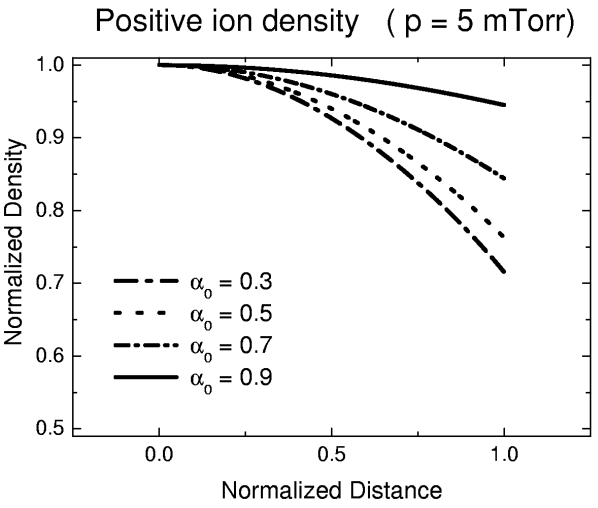

Fig. 4. Density profiles of positive ions at various α_0 (α_0 = 0.3, 0.5, 0.7, 0.9).

well with the relative radial distribution of the F density which was obtained by optical emission actinometry in SF_6 discharges [17] and CF_4 discharges [18]. The variation of the magnitude of the spatially averaged density of oxygen atoms with operating pressure was predicted by global modeling [13]. The oxygen atom density increases with pressure in the low-pressure range, and this was observed experimentally in an inductively coupled plasma [19] and a microwave discharge [6].

Figure 4 shows the density profiles of positive ions with varying α_0. As α_0 increases, the plasma uniformity improves. For a given pressure, the increase in α_0 is due to the decrease in input power. Therefore, at lower input power, the uniformity of charged species is better. Although not shown in figures, the density profile of negative ions has the same trend except that the decrease in the density along the distance is quite drastic at $\alpha_0 = 0.3$

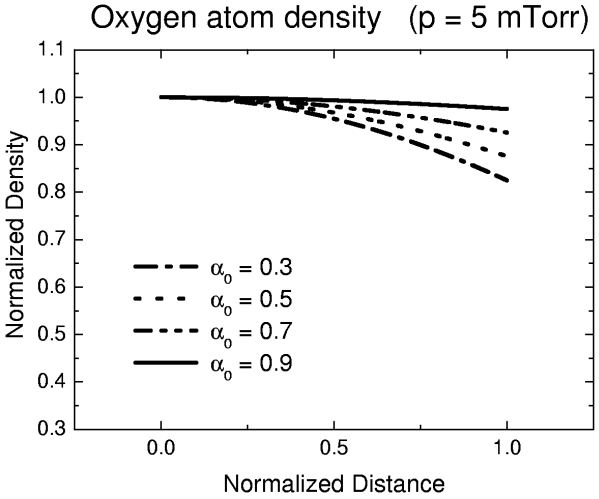

Fig. 5. Density profiles of oxygen atoms at various α_0 (α_0 = 0.3, 0.5, 0.7, 0.9).

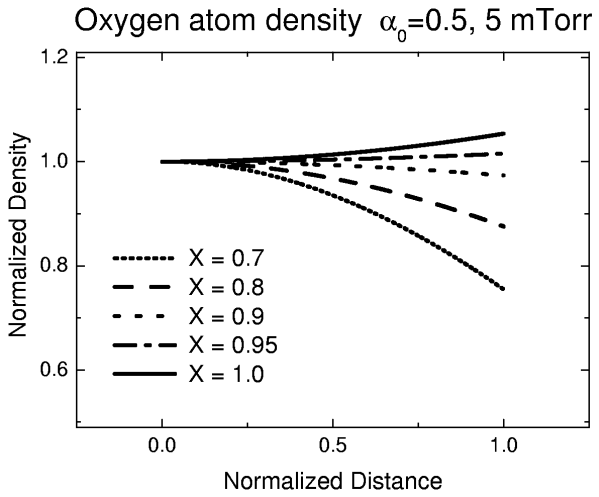

Fig. 6. Density profiles of oxygen atoms at various fractional dissociations X (X = 0.7 - 1.0).

and 0.5. Figure 5 shows the density profiles of oxygen atoms for various α_0. As α_0 increases, the uniformity of oxygen atoms improve. At lower input power, a better uniformity of oxygen atoms is achieved, as in the case of charged species.

Figure 6 shows the effect of the fractional dissociation on the density profiles of oxygen atoms. Whether the profile of oxygen atoms is parabolic (peaked in the plasma center) or hollow depends on the fractional dissociation X. As X approaches 1, the profile becomes hollow. As X decreases, the profile has a steeper down-slope. The fractional dissociation depends on the electron density and the electron temperature, which are determined by the operating pressure, the input power, and the reactor geometry. As the pressure increases, the fractional dissociation decreases; therefore, the profile of oxygen atoms has a shape peaked at the center.

IV. CONCLUSION

The equilibrium one-dimensional profiles of charged species and neutral atoms of high-density oxygen discharges are numerically calculated. The negative and positive ion concentrations in the bulk are assumed to be mostly determined by ionization, attachment, and recombination reactions. The simulation results compare well with experiments. The plasma uniformity is observed to degrade at higher pressure. The profiles of negative ions show stronger density gradients to the wall than those of positive ions. The profile of oxygen atoms is parabolic (peaked in the plasma center) or hollow, depending on the fractional dissociation. As the fractional dissociation approaches 1, the profile becomes hollow, and as it decreases, the profile has a steeper down-slope. High-density and large-area oxygen plasmas can be beneficial for process uniformity in industrial applications. Optical emission actinometry experiments are being performed to confirm the validity of this model.

ACKNOWLEDGMENTS

We are grateful to Professors A. J. Lichtenberg and M. A. Lieberman of the University of California at Berkeley for fruitful discussions. This work is supported by the Research Fund of Dong-A University (the program year of 2003).

REFERENCES

[1] S. Yun and G. R. Tynan, J. Appl. Phys. **89**, 911 (2001).
[2] T. Hori, M. D. Bowden, K. Uchino and K. Muraoka, J. Vac. Sci. Technol. A **14**, 144 (1996).
[3] C. Lee, D. B. Graves, M. A. Lieberman and D. W. Hess, J. Electrochem. Soc. **141**, 1546 (1994).
[4] T. H. Chung, L. Meng, H. J. Yoon and J. K. Lee, Jpn. J. Appl. Phys. **38**, 6890 (1999).
[5] H. J. Yoon and T. H. Chung, J. Korean Phys. Soc. **34**, 29 (1999).
[6] M. Naddaf, V. N. Bhoraskar, A. B. Mandale and S. R. Sainkar, Plasma Sources Sci. Technol. **11**, 361 (2002).
[7] S. Yun, K. Taylor and G. R. Tynan, Phys. Plasmas **7**, 3448 (2000).
[8] D. J. Economou, T. J. Bartel, R. S. Wise and D. P. Lymberopoulos, IEEE Trans. Plasma Sci. **23**, 581 (1995).
[9] K. Nanbu, T. Morimoto and M. Suetani, IEEE Trans. Plasma Sci. **27**, 1379 (1999).
[10] A. J. Lichtenberg, V. Vahedi, M. A. Lieberman and T. Rognlien, J. Appl. Phys. **75**, 2339 (1994).
[11] J. T. Gudmundsson, I. G. Kouznetsov, K. K. Patel and M. A. Lieberman, J. Phys. D: Appl. Phys. **34**, 1100 (2001).
[12] T. Mieno, K. Kamo, D. Hayashi, T. Shoji and K. Kadota, Appl. Phys. Lett. **69**, 617 (1996).

[13] H. J. Yoon and T. H. Chung, J. Korean Phys. Soc. **39**, 271 (2001).
[14] W. H. Press, S. A. Teukolsky, W. T. Vetterling and B. P. Flannery, *Numerical Recipes in C* (Cambridge University Press, New York, 1992).
[15] M. Yoon, S. C. Kim, H. J. Lee and J. K. Lee, J. Korean Phys. Soc. **32**, L635 (1998).
[16] St. Behle, A. Georg, Y. Yuan, J. Engemann and A. Brockhaus, Surf. Coat. Technol. **97**, 734 (1997).
[17] P. W. Lee, Y. J. Kim, C. S. Chang and H. Y. Chang, Rev. Sci. Instrum. **66**, 4591 (1995).
[18] M. Sarfaty, M. Harper and N. Hershkowitz, Rev. Sci. Instrum. **69**, 3176 (1998).
[19] D. C. Seo and T. H. Chung, J. Phys. D: Appl. Phys. **34**, 2854 (2001).